Fabrication of graphene oxide-reinforced polyvinyl alcohol and study effect of thermal annealing of GO/PVA nanocomposites on their properties

L. Gahramanli [a,b*], S. Bellucci [b], M. Muradov [a], M. B. Baghirov [a], S. Mammadyarova [a], G. Eyvazova [a], C. Vacacela Gomez [b]
[a] *Nano Research Laboratory, Excellent Center of Baku State University, Baku, Azerbaijan*
[b] *NEXT Laboratory, INFN, LNF, Frascati, Rome, Italy*

In the presented work, graphene oxide (GO) was obtained as a plate using the Hummer technique. X-ray diffraction (XRD) and Scanning Electron Microscopy (SEM) show the formation of pristine GO. Composite materials were prepared by adding different percentages of GO to polyvinyl alcohol (PVA) (2%GO/PVA, 3% GO/PVA, and 20% GO/PVA). To determine the effect of thermal annealing on the structure, physical properties, and morphology of the samples, thermal annealing of the samples was performed for 1 hour at temperatures (40°C, 70°C, and 110°C). Following that, to explore how the characteristics of GO/PVA composites vary with concentration and thermal annealing temperature, the structural, optical, and morphological features of the samples were determined using XRD, Fourier-transform infrared (FTIR), and Raman spectroscopy, as well as SEM used to investigate the properties of all samples. From the XRD results, by the increasing thermal annealing temperature, the space between the sheets is decreased. From Raman measurements, the I_D/I_G ratio for 2% and 3% GO/PVA composite materials increased with increasing temperature compared to the pristine GO. It indicates that the defect in the structure increases due to the effect of temperature.

(Received July 22, 2024; Accepted October 9, 2024)

Keywords: GO/PVA, Physical properties, Thermal annealing, Composite materials

1. Introduction

Carbon-based materials such as graphene and its related compounds have recently received significant interest in the field of science due to their extraordinary physical and chemical properties, particularly their zero-band gap, as mentioned in the literature [1,2]. Although its extraordinary characteristics graphene's absence of a band gap limits its active applications, relegating it to a passive position in electronic systems [3]. However, derivatives like GO and reduced graphene (rGO) have emerged as focal points of research due to their unique features. Unlike pristine graphene, GO possesses oxide groups, thereby introducing a distinct band gap [4,5]. Furthermore, GO's band gap can be finely controlled by strategically lowering these oxide groups, resulting in customized electrical properties [5-7]. Additionally, GO exhibits hydrophilic characteristics attributed to its carbonyl and carboxyl groups, facilitating effortless dispersion in aqueous environments [8-10]. The versatility of GO is exemplified by its applications in diverse fields, including drug delivery, solar energy conversion, and gas sensing, underscoring its main role in cutting-edge research and technology [11–13].

PVA, among the polymers compatible with GO, stands out due to its inherent biocompatibility and non-toxic nature, making it a material of choice for various applications. PVA finds widespread utility in fields such as fuel technology, coatings, and adhesives, owing to its desirable properties [14]. Also, due to its ability to easily form a layer and disintegrate, this material is used in drug delivery [15,16]. PVA has many hydroxy groups, which makes it useful for creating porous structures [17]. In this regard, PVA is used in the creation of many membranes [18]. Incorporating GO into the PVA matrix initiates substantial transformations in its physical and chemical characteristics. Precise control over the optical, electrical, and structural features of GO/PVA composites is achievable by manipulating the weight percentage of incorporated GO.

* Corresponding author: gahraman.lala@gmail.com
https://doi.org/10.15251/JOR.2024.205.715

Research findings indicate that an increase in GO content enhances the composite's crystallinity while concurrently narrowing its band gap, resulting in materials with tailored electronic properties [19,20]. Kashyap, S et al. experiments show that adding 0.3 wt% GO to PVA results in a 150% increase in modulus of elasticity [21]. These composite materials exhibit exceptional resilience, enduring rigorous processes such as thermal treatment and exposure to gamma radiation, leading to a spectrum of property modifications [22-24]. Notably, the incorporation of GO reinforces the mechanical strength. It augments the thermal stability of PVA, making these composites exceptionally well-suited for advanced applications, including Schottky structures, supercapacitors, and air purification filters [25–29].

Despite the extensive body of research on various aspects of GO/PVA composites, an in-depth comprehension of the modifications caused by thermal annealing processes remains an important knowledge gap. The present research aims to fill this gap through inquiry into the subtle variation of physical properties of GO/PVA composites with varying weight concentrations (2, 3, and 20 wt%) at different thermal treatment temperatures (40°C, 70°C, and 110 °C). Through systematic experimentation and analysis, this research aims to elucidate the intricate relationship between thermal processing parameters and the resulting material properties, thereby contributing valuable insights to the burgeoning field of advanced materials science.

2. Materials and methods

In this research utilized a modified Hummer's approach to synthesis GO [30,31]. Graphite powder (3 g) and $NaNO_3$ (1.5 g) had previously been mixed in a 500 mL reaction flask. Following that, 70 mL of concentrated H_2SO_4 was progressively incorporated into the solution at a slow rate while cooling in an ice bath and stirring for an hour. Then, $KMnO_4$ was gradually introduced into the solution in phases, causing a rapid increase in reaction temperature. It was critical to keep the reaction temperature under 20 °C for the whole three-hour operation. The mixture was then removed from the ice bath and agitated for an hour at 35°C. The solution concentrated and reached a temperature of 98 °C when 150 mL of water was introduced gradually. This temperature was kept for 30 minutes. The mixture was agitated for an hour after slowly adding the solution to 300 mL of water. After introducing 15 mL of 30% H_2O_2 to the mixture, it was agitated for 30 minutes. After that, the mixture was filtered through filter paper, washed with a 1:10 HCl: distilled water mixture (250 mL) to remove any remaining metal ions, and allowed to air dry at ambient temperature [32,33].

After being diluted with distilled water, the final substance was exposed to ultrasounds. It was then filtered and precipitated in a centrifuge, and the resulting material was dried at ambient temperature.

Distilled water was chosen as the solvent for PVA due to its appropriateness. The dispersion of GO nanostructures in water is facile, enabling the use of water as a medium. Initially, distilled water was used to mix a predetermined quantity of PVA to create a concentrated solution that was 5%. The polymer was completely dissolved in the solution using a magnetic stirrer. Subsequently, the combination was subjected to ultrasound after introducing GO to this mixture for two minutes. After filtering the mixture with various quantities of mass into petri dishes, it was allowed to dry at room temperature. It is significant to remember that GO was added in concentrations of 2%, 3%, and 20% throughout the production of the final composites.

Utilizing the Rigaku Miniflex equipment, the samples' X-ray structural analyses were examined. For the analysis of Raman spectra, an InVia microscope Renishaw, to get FTIR spectra was used Agilent Cary 630 FTIR Spectrometer. To investigate the morphological properties of nanocomposite materials Vega II microscope Tescan was used.

3. Result and discussion

3.1. Structure of pristine GO

Figure 1 depicts XRD analysis (Fig.1.a) and TEM images (Fig.1.b) of GO produced using the Hummer method. The XRD spectrum of pristine GO from Fig. 1.a revealed three diffraction peaks at $2\theta = 11.98°$, 26.30°, and 42.04°, reflecting the (001), (002), and (100) planes, respectively.

Fig. 1.b depicts TEM images of GO in its pristine state. From this, it is clear that GO is made up of multiple layers. The results reveal that GO synthesized using the Hummer technique was successfully produced.

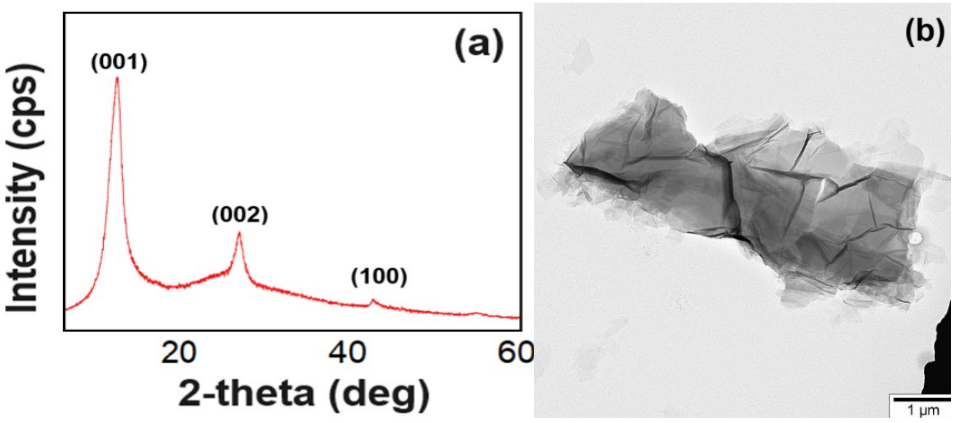

Fig. 1. Pristine GO: a) XRD pattern and b) TEM images.

3.2. XRD results

The impacts of various temperatures (25 °C, 40 °C, 70 °C, and 110 °C) on the PVA polymer matrix, which was utilized as the initial matrix in the samples, were ascertained using XRD assessment. It was found that, on average, the annealing temperature enhanced together with the degree of crystallinity of PVA [20]. Thermal annealing is performed at temperatures of 40°C, 70°C, and 110°C after the manufacture of various concentrations of GO/PVA nanocomposite materials (2%, 3%, and 20%). The thermal annealing of GO/PVA nanocomposites generated at the respective concentrations yielded the XRD spectra shown in Figure 2.

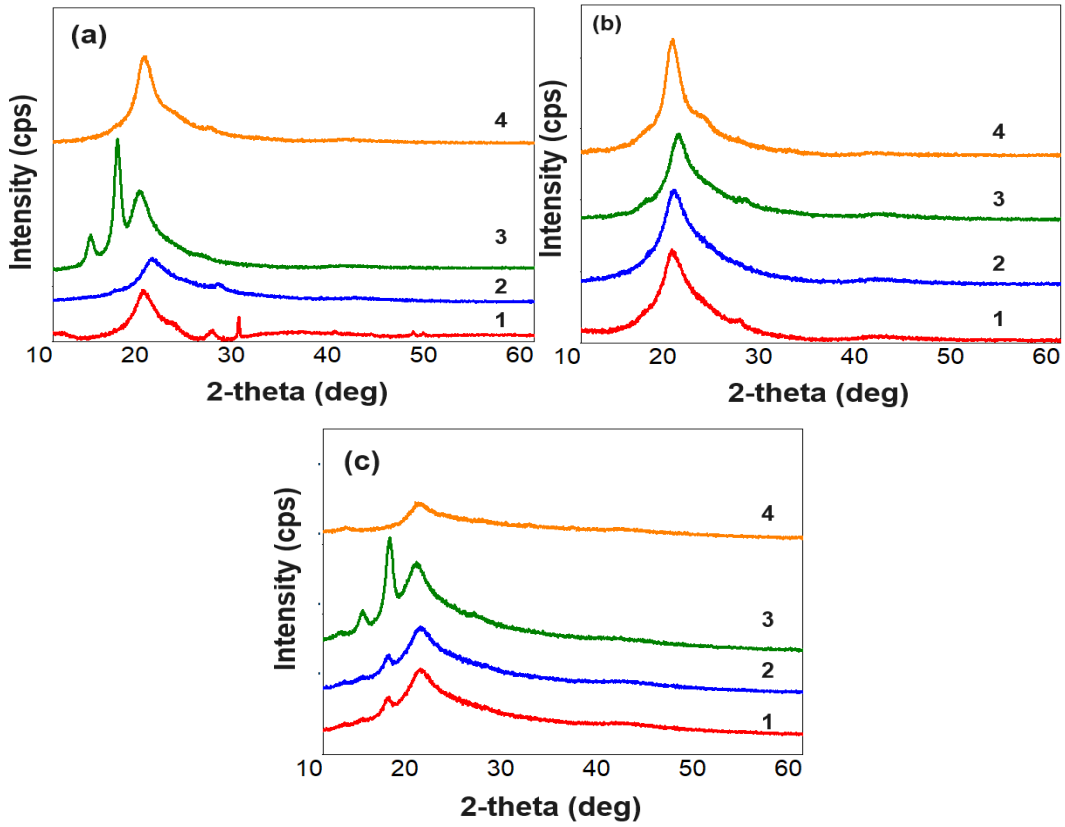

Fig. 2. XRD analysis of a) 2% GO/PVA nanocomposite materials; b) 3% GO/PVA nanocomposite materials; c) 20% GO/PVA. nanocomposite materials at different annealed temperatures 1-T=25°C, 2-T=40°C, 3-T=70°C, 4-T=110°C.

XRD pattern of 2% GO/PVA, 3% GO/PVA, and 20%GO/PVA is demonstrated in Fig.2. a, b, and c, respectively. These samples performed thermal annealing at 40°C (2), 70°C (3), and 110°C (4) in addition to being studied at ambient temperature (1-T=25°C). In the pattern of 2% GO/PVA composite formed at ambient temperature and thermally treated composites at T = 40 °C, T = 70 °C, and T = 110 °C, respectively, the diffraction peaks are found at 2θ=19.67°, 19.43°, 20.30°, and 19.67° corresponding to (101) plane. These peaks belong to PVA. Here, the typical GO peak (2θ = 10.6°) is not seen, and the missing of this peak suggests that GO is evenly distributed throughout the PVA. Moreover, all samples exhibit a peak at approximately 2θ = 26°, which is associated with the (002) reflection plane. This peak is associated with graphite, the first substance that was chosen. The process of the PVA softening as temperature rises is shown in Fig.2. a, b, and c. This leads to the production of the distinctive little intensity peaks connected to PVA. All samples exhibit newly oriented structures inside the PVA polymer matrix and GO at temperatures of 40°C and 70°C. The polymer's vitrification process begins at 110°C.

The GO characteristic peaks are not found in these nanocomposite materials. This is because the GO layers are spread inside the PVA. Consequently, the signals belonging to the GO are lost in the backdrop of the signals belonging to the PVA polymer matrix.

3.3. Raman spectroscopy

An effective method for analyzing structural alterations in carbon-based materials is Raman spectroscopy. The Raman spectrum of pristine PVA (Fig. 3.a) and GO (Fig.3.b) are displayed in Figure 3. From Fig. 3.a, typical peaks belonging to pristine PVA are observed [34, 35]. Fig. 3.b illustrates, that the wave numbers of 1352.64 cm^{-1} and 1604.08 cm^{-1} related to the D band are defined by sp^3 hybridized carbon, and the G bands by sp^2 hybridized carbon, respectively. To determine the defects in the structure, it is necessary to determine the I_D/I_G ratio. This will allow us to analyze the quality of the formed structure [36]. For pristine GO, this value is equal to 0.933. Fig.3.c shows the Raman spectrum of a 2% GO/PVA composite material at various temperatures. At ambient temperatures, the 2% GO/PVA composite showed two primary GO bands. The D band at 1352.63 cm^{-1} was caused by structural flaws and disorganization in graphene, whereas the G band at 1605.68 cm^{-1} was caused by the stretching of the C-C bond in graphitic materials [37]. This sample has a D/G intensity of bands ratio (I_D/I_G) of 0.912. Table 1 shows the exact location of the D and G bands, as well as the I_D/I_G ratios, for composites made from PVA and GO at various concentrations. As shown in Table 1, the D peak shifts from 1352.63 cm^{-1} to 1360.86 cm^{-1} for 2% GO/PVA composite with a temperature rise from 25°C to 110°C. The slight shift of this peak to a higher wavenumber was observed for this composite annealed at 110°C.

In the Raman spectra of 3% (Fig.3.d) and 20% GO/PVA (Fig.3.e) composite, as temperatures rise, the D and G peaks gradually move to greater wavenumbers. For all samples, the peaks observed for the D and G bands are shifted towards a large wavenumber. The obtained spectra show a divergence at 70°C annealing temperature.

Thus, the I_D/I_G ratio at 70°C calculated in Table 1 received the greatest value for all percentages. This is considered to be related to PVA's glass transition temperature.

Qualitatively, in 2% and 3% GO/PVA composite materials, the I_D/I_G ratio increased with increasing temperature compared to the original GO. This indicates that the defect in the structure increases due to the influence of temperature. However, it can be noted that defect structures are reduced and more regular carbon structures are formed in 20% GO/PVA composite materials compared to the original GO.

Table 1. D and G peaks position observed in Raman spectra and (I_D/I_G) ratios for composites based on 2%, 3%, and 20% GO/PVA.

Composite materials		**D peak position (cm^{-1})**	**G peak position (cm^{-1})**	**I_D/I_G**
2% GO/PVA	25°C	1352.63	1605.68	0.912
	40°C	1355.97	1604.07	0.911
	70°C	1350.96	1605.68	0.945
	110°C	1360.86	1605.57	0.932

Composite materials		D peak position (cm^{-1})	G peak position (cm^{-1})	I_D/I_G
3% GO/PVA	25°C	1349.28	1604.07	0.942
	40°C	1354.30	1605.68	0.944
	70°C	1355.97	1605.68	0.953
	110°C	1357.52	1607.18	0.941
20% GO/PVA	25°C	1353.04	1570.31	0.825
	40°C	1337.57	1605.68	0.887
	70°C	1345.94	1592.75	0.895
	110°C	1367.54	1605.57	0.827

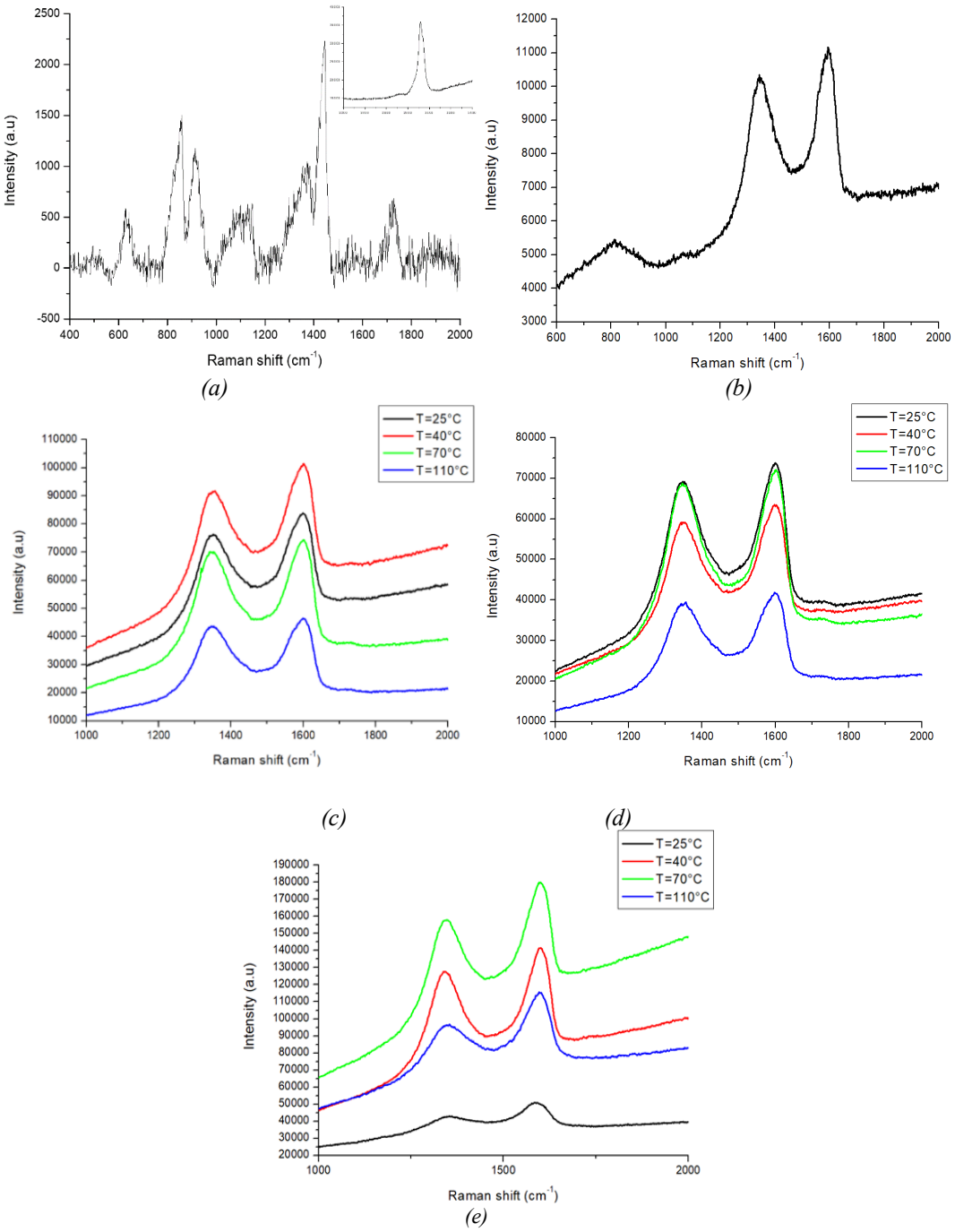

Fig. 3. Raman spectrum of pristine a) PVA, b) GO, and in different thermally annealing temperatures of c) 2% GO/PVA, d) 3% GO/PVA, e) 20% GO/PVA.

The I_d/I_g ratio given in Table 1 for all samples allows for determining the defect structures present in their crystal structure depending on the temperature. So, as a rule, the I_d/I_g ratio increases up to 70°C for all samples, and this ratio decreases at the next temperature increase (110°C). That is, the increase of defect structures at high temperatures is related to the melting (softening) of PVA polymer, amorphization happens when the composite material crystal structure contains a substantial number of flaws. This is also reflected in the XRD results. Thus, the characteristic PVA peak observed in the XRD pattern for all samples at low temperatures slightly decreases at high temperatures, however, the intensity reduces significantly in the 20% GO/PVA combination.

3.4. FTIR spectroscopy

FTIR spectroscopy was used to assess whether functional chemical groups existed in the composite materials. FTIR spectrum of pristine PVA (Fig.4.a) and GO (Fig.4.b) is demonstrated in Figure 4.

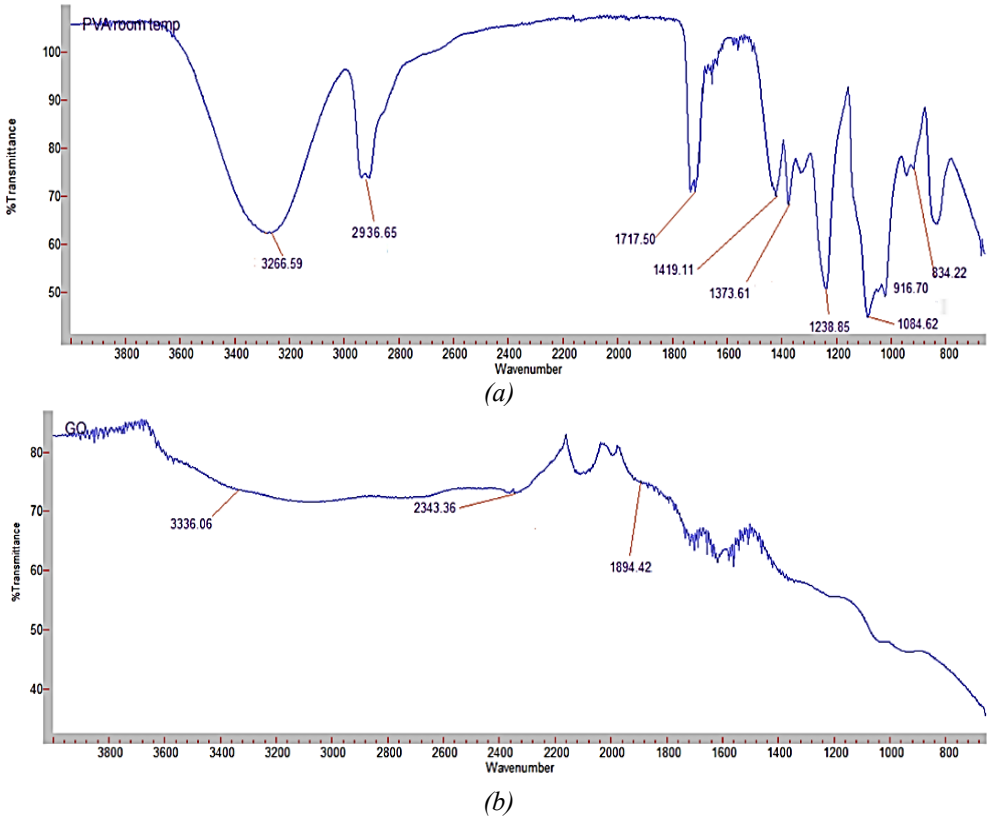

Fig. 4. FTIR spectrum of pristine a) PVA and b) GO.

In the FTIR spectrum of pristine PVA, the peak at 3266.59 cm^{-1} is attributed to the -OH stretching vibration [38]. The peak seen at 2936.65 cm^{-1} corresponds to the asymmetric stretching of CH_2 at 2906 cm^{-1} [39]. The band at 1717.50 cm^{-1} corresponds to the stretching vibrations of C=O [38]. 1419.11, 1373.61, 1084.62, 916.70, and 834.22 cm^{-1} are corresponding to CH_2 bending, δ (OH), rocking with CH wagging, stretching of C-O and bending of OH (amorphous sequence of PVA), CH_2 rocking and C-C peaks due to stretching, respectively. The literature identifies 1084 and 1024 cm^{-1} as crystallization-sensitive bands related to C-O stretching oscillations [40]. The peak observed at 1238.85 cm^{-1} is also related to functional groups belonging to PVA (C–H wagging mode) [40].

Fig. 4.b illustrates the FTIR spectrum of pristine GO. Here, the broad peak observed at 3336.06 cm^{-1} is associated with C–OH oscillation from COOH and H_2O [41], and the bands that occurred at 2343.36 and 1894.42 cm^{-1} are connected with CO_2 and C=O, respectively [41]. The

typical peaks of GO mainly found from 2800 to 2900 cm^{-1} are related to both asymmetric and symmetric CH_2 stretching of GO. However, since the band attributed to the C-OH groups in Fig.4. b is broad, it is assumed that the relatively weak peaks attributed to CH_2 are lost in the background of the C-OH bond [42].

Figure 5 depicts the FTIR spectrum of different concentrations of GO/PVA (2%, 3%, and 20%) at T=25°C.

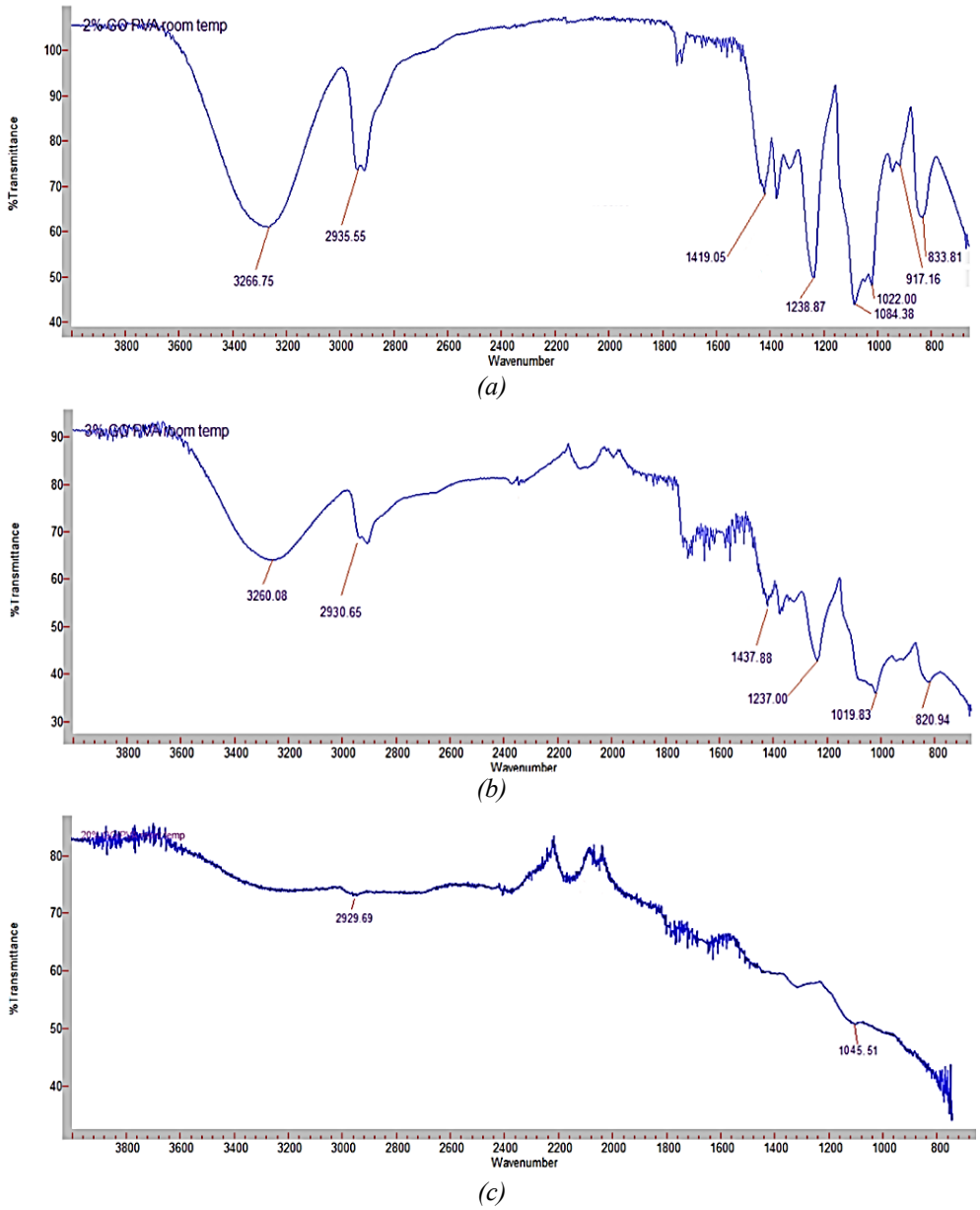

Fig. 5. FTIR spectrum of a) 2%GO/PVA; b) 3%GO/PVA and c)20% GO/PVA composite materials at T=25°C.

Peaks at ~3300 cm^{-1} in the FTIR spectra of 2% GO/PVA (Fig.5.a), 3% GO/PVA (Fig.5.b), and 20% GO/PVA (Fig.5.c) composite materials at ambient temperature indicate O-H stretching. So, this peak is 3266.75 cm^{-1} for 2% GO/PVA nanocomposite, at 3260.08 cm^{-1} for 3% GO/PVA, and for 20%GO/PVA, this peak is a more amorphous form and a wide transmittance was observed [43]. This is explained by a significant increase in GO content in the PVA, as well as a decrease in the oscillation frequency of the distinctive OH groups.

The observed peak at 2935.55 cm^{-1} in Fig. 5.a, 2930.65 cm^{-1} in Fig. 5.b, and 2929.69 cm^{-1} in Fig. 5.c is related to the asymmetric CH_2 group stretching oscillation [44]. The weakening of this band and the shift to lower frequencies with increasing concentration of GO in PVA demonstrates the reduction of the oscillation frequencies of functional groups, in other words, the association of GO's hydroxyl and carboxyl groups to PVA. The fact that this bending is more intense and observed in small percentages and this bending becomes weaker with increasing concentration demonstrates the weak bending between PVA and GO. At the same time, the detected bands in the 2800-2900 cm^{-1} region are scissor-shaped and correspond to asymmetric and symmetric CH_2 stretching. Asymmetric peaks were observed in the FTIR spectrum of low-concentration composite materials and their intensity reduced as concentration increased, however in nanocomposites with a higher concentration, the scissor-shaped peak disappeared as broadband and the peak's intensity fell (the symmetrical band was not detected).

1419.06 cm^{-1} and 1238.87 cm^{-1} in Fig.5. a. are the related couplings of PVA chains cause in-plane O-H vibration, while C-H wagging vibration [45]. In 3% GO/PVA composite materials (Fig. 5.b), these peaks are observed at 1237.00 and 1437.88 cm^{-1}. In 20% GO/PVA composite materials, these bending are lost. That is, the weakening of the intensity of the bending between GO and PVA with increasing concentration, and the fact that these functional groups are not observed at higher concentrations indicates the weakening of hydrogen bonds between the hydroxyl groups in PVA molecules and functional groups that include oxygen of GO.

All the peaks observed at 1084.38, 1022.00, 917.16 cm^{-1}, and 833.81 cm^{-1} in Fig.5.a correspond to the PVA. The characteristic bands at 1237.00, 1019.83, and 820.94 cm^{-1} are observed in Fig.5. b, and only the band at 1045.51 cm^{-1} is seen in Fig. 5.c. With increasing amounts of GO within the composite material, the bands belonging to PVA weakened or disappeared [46].

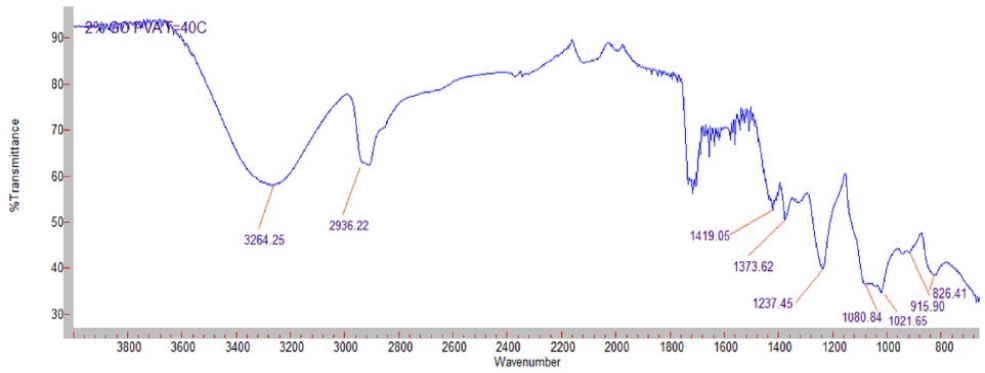

(a)

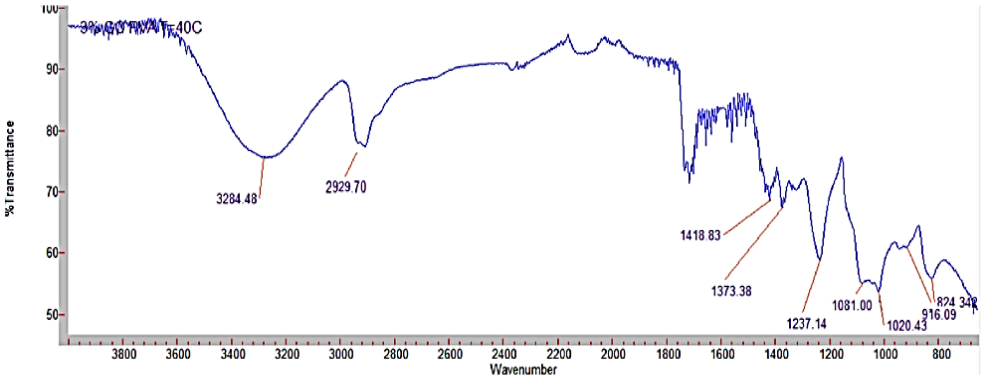

(b)

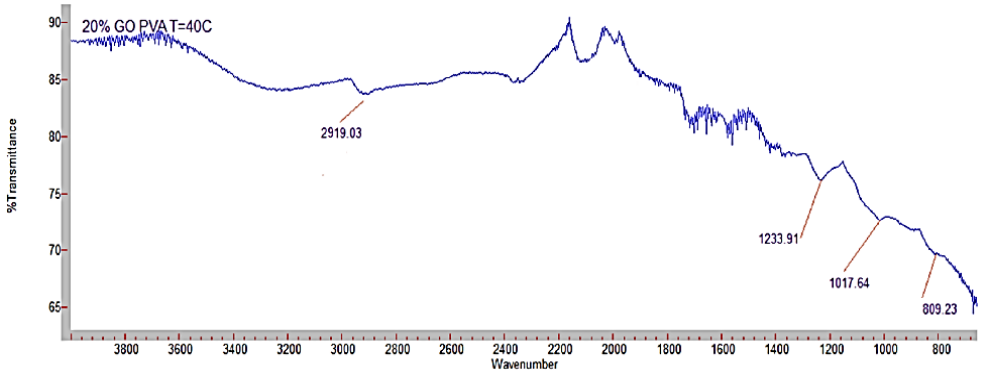
20% GO PVA T=40C
%Transmittance
Wavenumber
2919.03
1233.91
1017.64
809.23

(c)

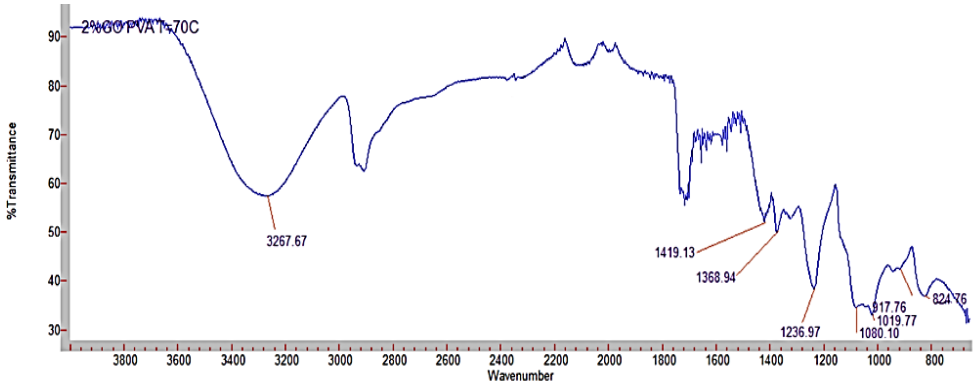
%Transmittance
Wavenumber
3267.67
1419.13
1368.94
1236.97
1080.10
917.76
1019.77

(d)

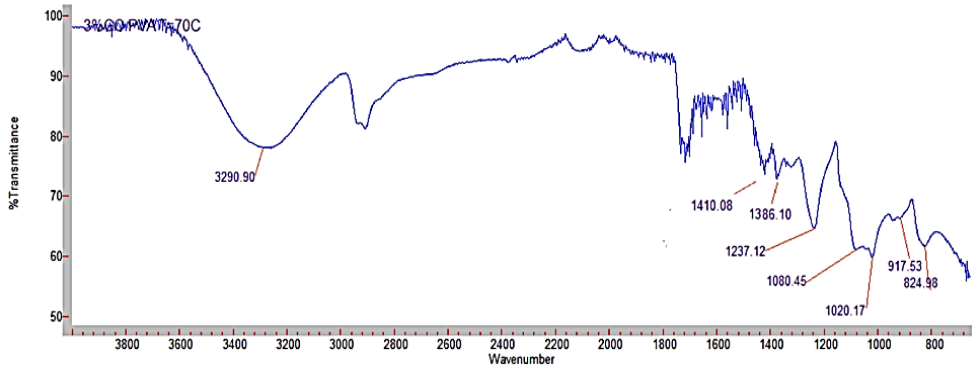
%Transmittance
Wavenumber
3290.90
1410.08
1386.10
1237.12
1080.45
1020.17
917.53
824.98

(e)

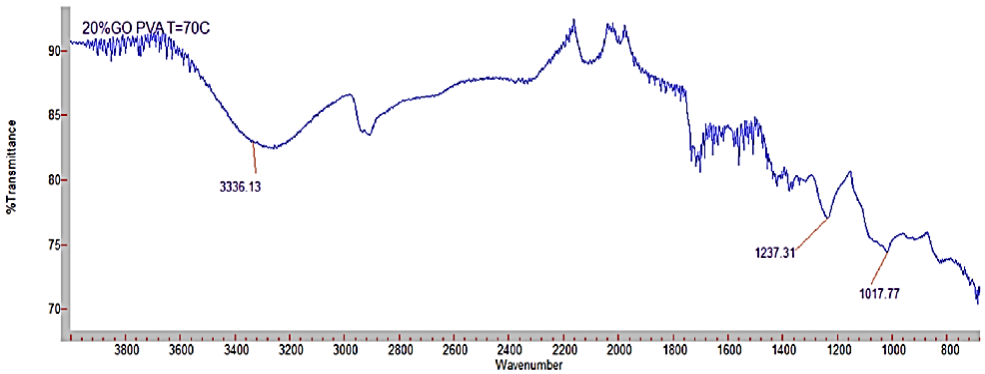
20%GO PVA T=70C
%Transmittance
Wavenumber
3336.13
1237.31
1017.77

(f)

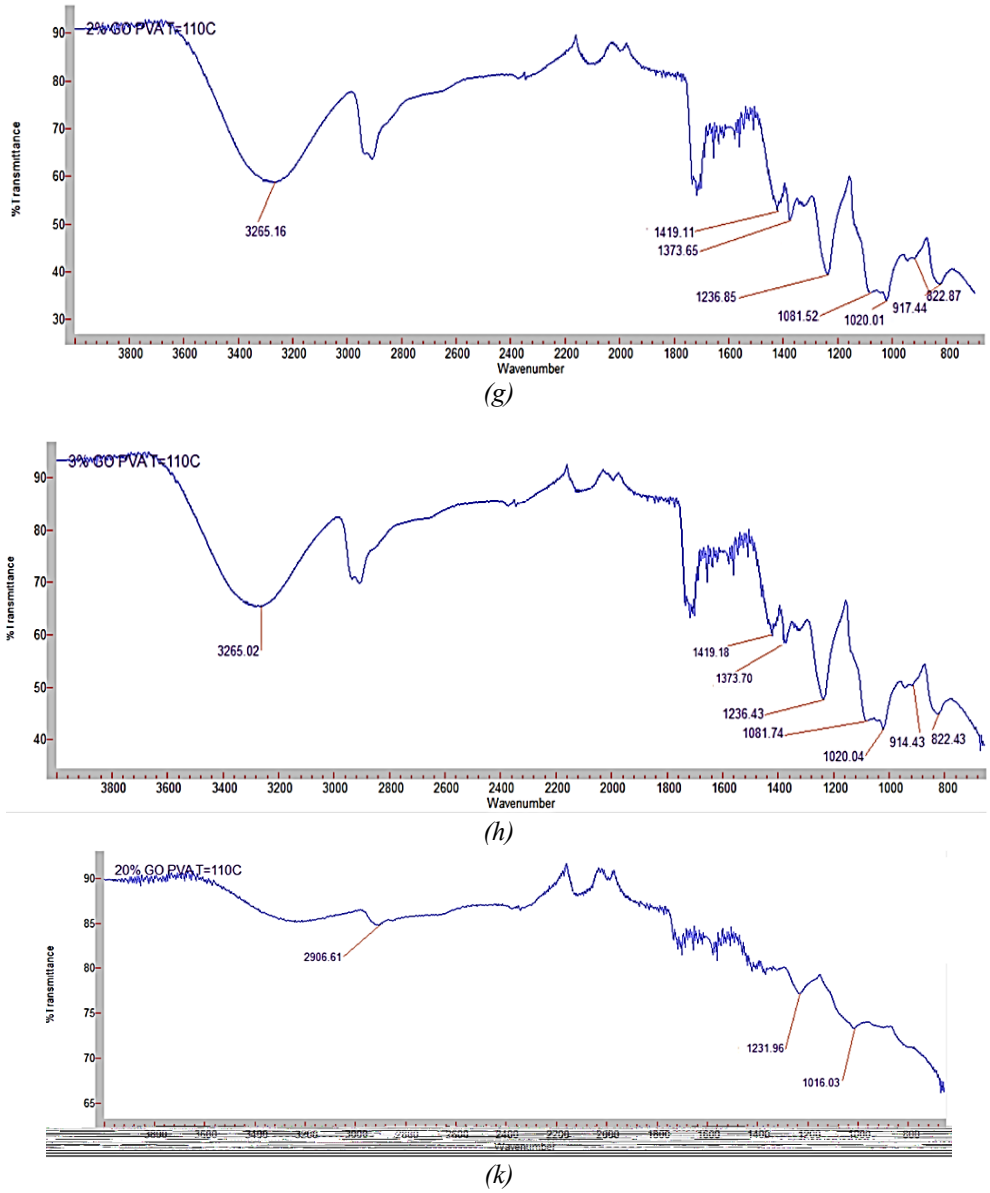

Fig. 6. FTIR spectrum of a) 2% GO/PVA, b) 3% GO/PVA, c) 20% GO/PVA composite materials thermally annealed at 40°C and d) 2%GO/PVA, e) 3% GO/PVA, f) 20% GO/PVA thermally annealed at 70°C and g) 2% GO/PVA, h) 3% GO/PVA, k) 20% GO/PVA thermally annealed at 110°C.

Figure 6 demonstrates the FTIR spectrum of 2% GO/PVA (Fig.6.a), 3% GO/PVA (Fig.6.b), 20% GO/PVA (Fig.6.c) nanocomposites thermally annealed at 40°C and 2% GO/PVA (Fig.6.d), 3% GO/PVA (Fig.6.e), 20% GO/PVA (Fig.6.f) nanocomposites thermally annealed at 70°C and 2% GO/PVA (Fig.6.g), 3% GO/PVA (Fig.6.h), 20% GO/PVA (Fig.6.k) nanocomposites thermally annealed at 110°C.

Here, 826.41, 915.90, 1021.65 and 1080.84 cm^{-1} peaks belong to the PVA. In the spectrum of 3% GO/PVA composite materials, the intensity of these peaks was somewhat weakened and appeared at 824.34, 916.09, 1020.43, and 1081.00 cm^{-1}. With the increase in concentration, some of these peaks disappeared and only peaks at 809.23 cm^{-1} and 1017.65 cm^{-1} were found.

The observed bands at 1237.45, 1373.62, and 1419.05 cm^{-1} correspond with bending and wagging of CH_2 vibrations [47] in Fig. 6.a. These peaks were observed at 1237.14, 1373.38, and 1418.83 cm^{-1} for 3% GO/PVA composite (Fig.6.b), this band was seen at 1233.91 cm^{-1} in the 20% GO/PVA combinations (Fig. 6.c).

The scissor-shaped peaks found at 2920 cm^{-1} for all three concentrations (2936.22 cm^{-1}, 2929.70 cm^{-1}, and 2919.03 cm^{-1}) are caused by asymmetric C-H stretching vibration bonds. As the amount of GO in the composite material enhanced, the peak intensity diminished. By the same rule,

the absorptions observed at 3264.25 cm^{-1} and 3284.48 cm^{-1} are linked to the intermolecular hydrogen bond of PVA.

Thermally annealed at 70°C of 2% GO/PVA composite material the peaks at 824.76 cm^{-1}, 917.76 cm^{-1}, 1019.77 cm^{-1}, and 1080.10 cm^{-1} (Fig.6.d), for 3% GO/PVA composite material the bands at 824.98, 917.53 cm^{-1}, 1020.17 cm^{-1}, 1080.45 cm^{-1} (Fig.6.e), for 20%GO/PVA composite material the peaks at 1017.77 cm^{-1} are related to the PVA (Fig.6.f). CH_2 wagging and bending peaks in the spectrum of 2%GO/PVA are at 1236.97, 1368.94, and 1419.13 cm^{-1}. These characteristic peaks are at 1237.12, 1386.10, and 1410.08 cm^{-1} in the spectra of 3% GO/PVA and the only bands at 1237.31 cm^{-1} are observed in the spectrum of 20% GO/PVA.

In the thermally annealed at 110°C, the peaks related to PVA are at 822.87, 917.44, 1020.01, 1081.52 cm^{-1} for 2% GO/PVA (Fig. 6.g), 822.43, 914.43, 1020.04, 1081.74 cm^{-1} for 3% GO/PVA (Fig. 5.h), for 20% GO (Fig. 6.k) is observed at 1016.03 cm^{-1}. The peaks related to CH_2 wagging and bending are observed at 1236.85, 1373.65, 1419.11 cm^{-1} for 2% GO/PVA, 1236.43, 1373.70, 1419.18 cm^{-1} for 3% GO/PVA, and only at 1231.96 cm^{-1} for 20% GO/PVA. The peaks attributed to C-H stretching vibration located at about 2900 cm^{-1} are seen in all 3 composite materials, but with the increase in concentration, the intensity of these scissor-shaped peaks weakened. The band is indicated at 2906.61 cm^{-1} for the 20% GO/PVA composite material.

According to the results obtained from the FTIR spectrum of the thermally annealed samples, it can be noted that the band intensities associated with PVA decreased with the increase in the amount of GO within the composite material. In contrast, some peaks completely disappeared at the highest concentration (20%). However, even when thermal annealing at the highest temperature, the structure of these composite materials did not change, the relationship between GO and PVA was maintained for all samples, although the intensities were weakened.

3.5. Morphological analysis

The morphology of all the samples was investigated at thermal annealing temperatures to observe changes in the surface structures of the samples. Figure 7 shows pictures of thermally annealed pristine PVA at various temperatures (40°C-Fig.7.a,70°C- Fig.7.b, and 110°C- Fig.7.c).

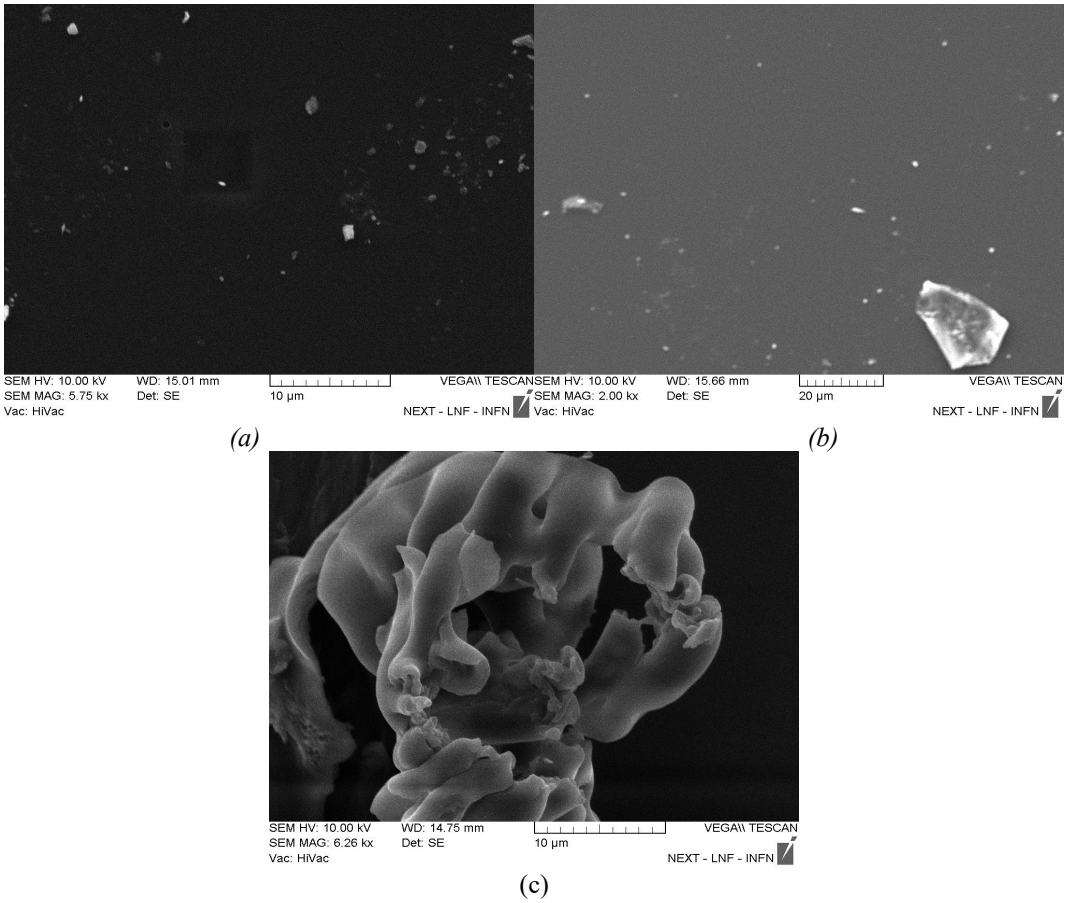

Fig. 7. SEM images of PVA thin film a) at 40°C; b) at 70°C; c) at 110°C.

Fig.7.c clearly shows that thermal annealing of pristine PVA at 110°C causes a fundamental alteration in the morphology of PVA. As a result of the temperature influence, PVA is broken down and its complete structure is destroyed.

The surface morphology of 2% GO/PVA samples prepared at T=25°C (Fig. 8. a), 40°C (Fig.8. b), 70°C (Fig. 8. c), and 110°C (Fig. 8.d) thermally annealed samples are shown in Figure 8.

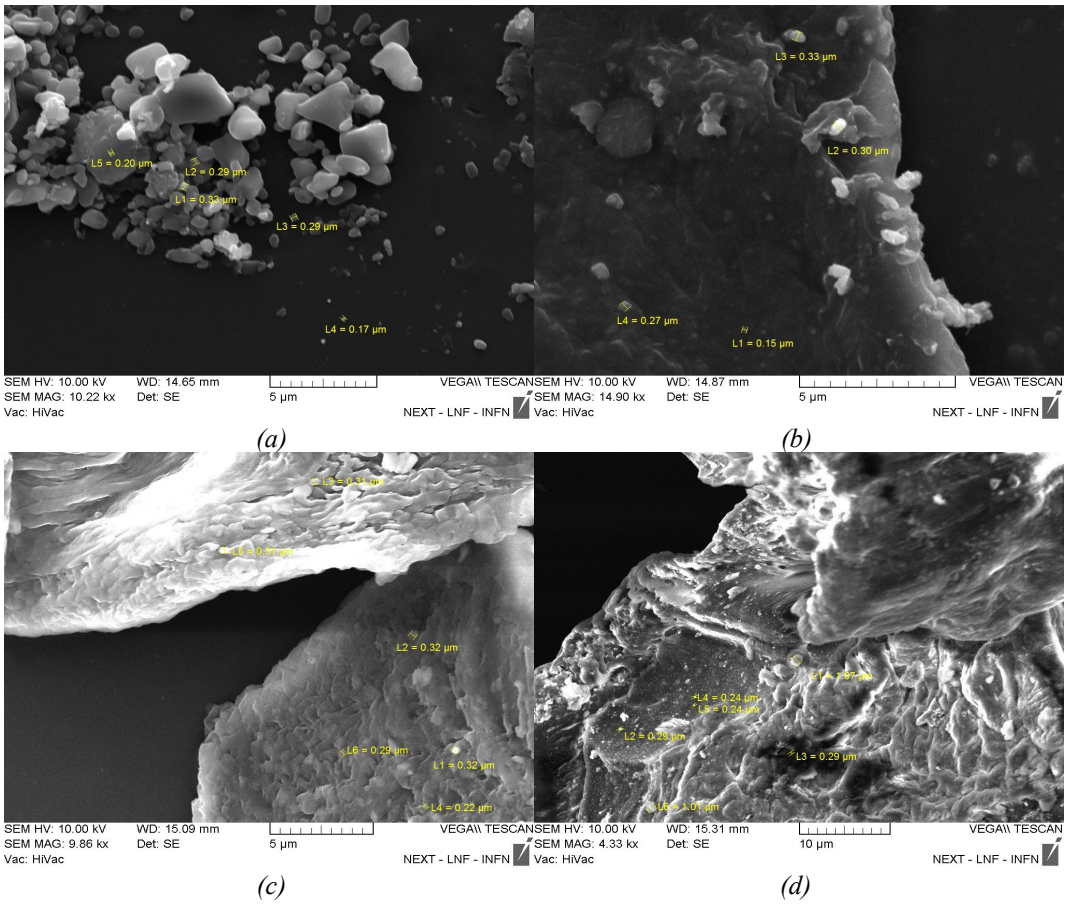

Fig. 8. SEM images of 2% GO/PVA Composite: a) at T=25°C; b) at 40°C; c) at 70°C and d) at 110°C.

The SEM image of the 2% GO/PVA sample at T=25°C shows the production of crystallites of varying sizes on the PVA polymer matrix's surface. Large-sized crystallites were created alongside small-sized crystallites. Small crystallites with diameters ranging from 0.17 µm to 0.33 µm combined to produce massive agglomerates. Note that the formed crystallites were formed on the smooth surface of the PVA.

The temperature effect caused Fig.8. b shows abnormalities on the smooth surface of the PVA, with tiny crystallites measuring between 0.15 and 0.33 µm in size. The surface of PVA roughened up at the following temperature increase of 70°C; these dimensions fell between 0.22 and 0.32 µm. The PVA was entirely disrupted in the morphology of the samples obtained by annealing at 110°C, and the size of the crystallites found on its surface was found to be between 0.24 µm and 1.07 µm.

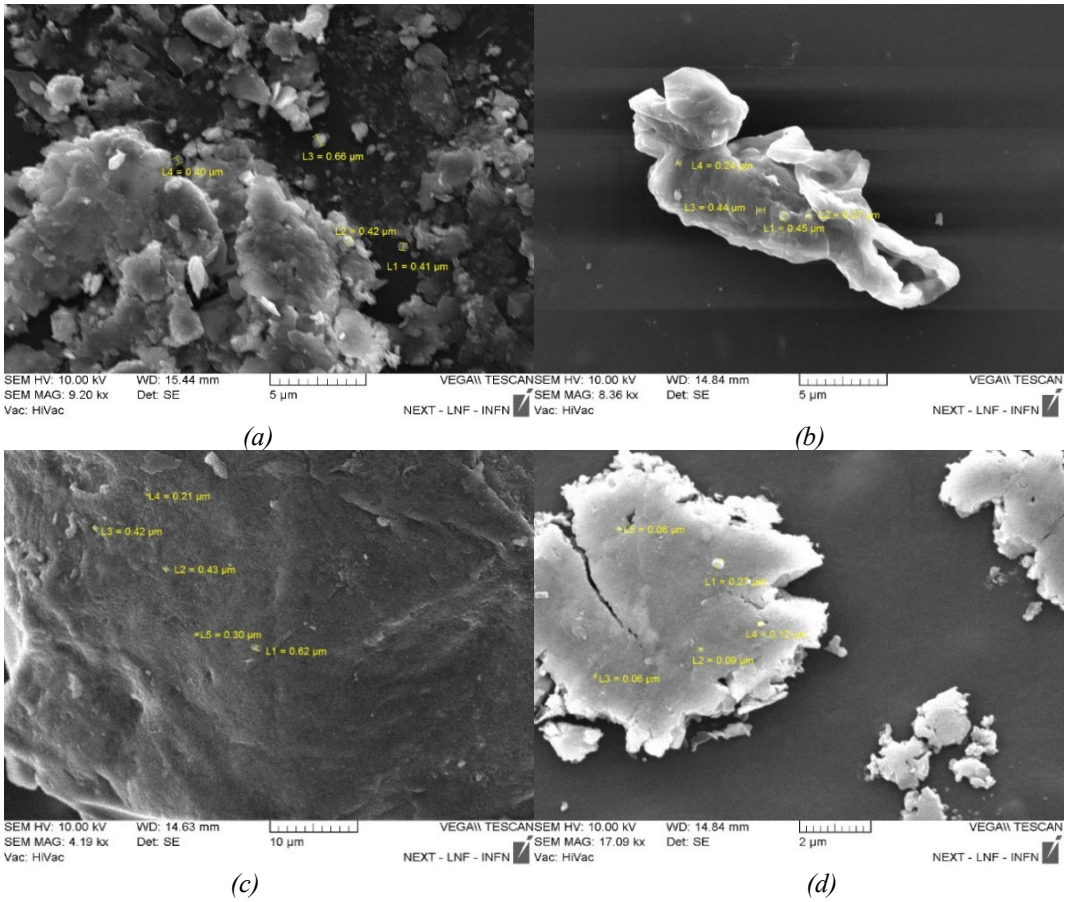

Fig. 9. SEM images of 3% GO/PVA Composite: a) at T=25°C; b) at 40°C; c) at 70°C; d) at 110°C.

SEM images of 3% GO/PVA samples prepared at T=25°C (Fig. 9. a), 40°C (Fig.9. b), 70°C (Fig. 9. c), and 110°C (Fig. 9.d) thermally annealed samples are illustrated in Figure 9. The layered structure of GO is positioned on the PVA polymer matrix surface, and its diameters range from 0.40 µm to 0.66 µm, as established by the morphology of the samples obtained from the synthesis of 3%GO/PVA at T=25°C (Fig.9. a). The temperature effect caused the PVA polymer matrix to alter in nanocomposite materials that were thermal annealed at 40°C, and the diameters of GO were found to be between 0.24 and 0.45 µm (Fig.9. b). The diameters of GO were found to be 0.21 µm -0.62 µm from SEM image of nanocomposite materials thermal annealed at 70°C (Fig.9. c). The following temperature rise, 110°C, caused GO to form massively on the surface of PVA. The dimensions of the GO 2D structure that resulted were found to be between 0.06 µm and 0.27 µm (Fig.9.d). From this, it can be seen that the temperature had an impact on the GO layers, causing them to divide into smaller-sized layers.

SEM pictures of 20% GO/PVA nanocomposite materials are demonstrated in Figure 10. The morphology of samples annealed at 40°C is displayed in Fig. 10. a. On the PVA polymer matrix surface, GO nanomaterials with a diameter of 0.19–0.43 µm were created. Temperature caused GO nanoparticles in crystallite form to scatter and cover the PVA polymer matrix's surface. Their dimensions of thermally annealed at 70°C of 20% GO/PVA nanocomposite materials (Fig.10.b) were found to be between 0.14 and 0.40 µm. The particle size of thermally annealed at 110°C of 20% GO/PVA (Fig.10.c) is between 0.19 and 0.45 µm, according to the SEM picture.

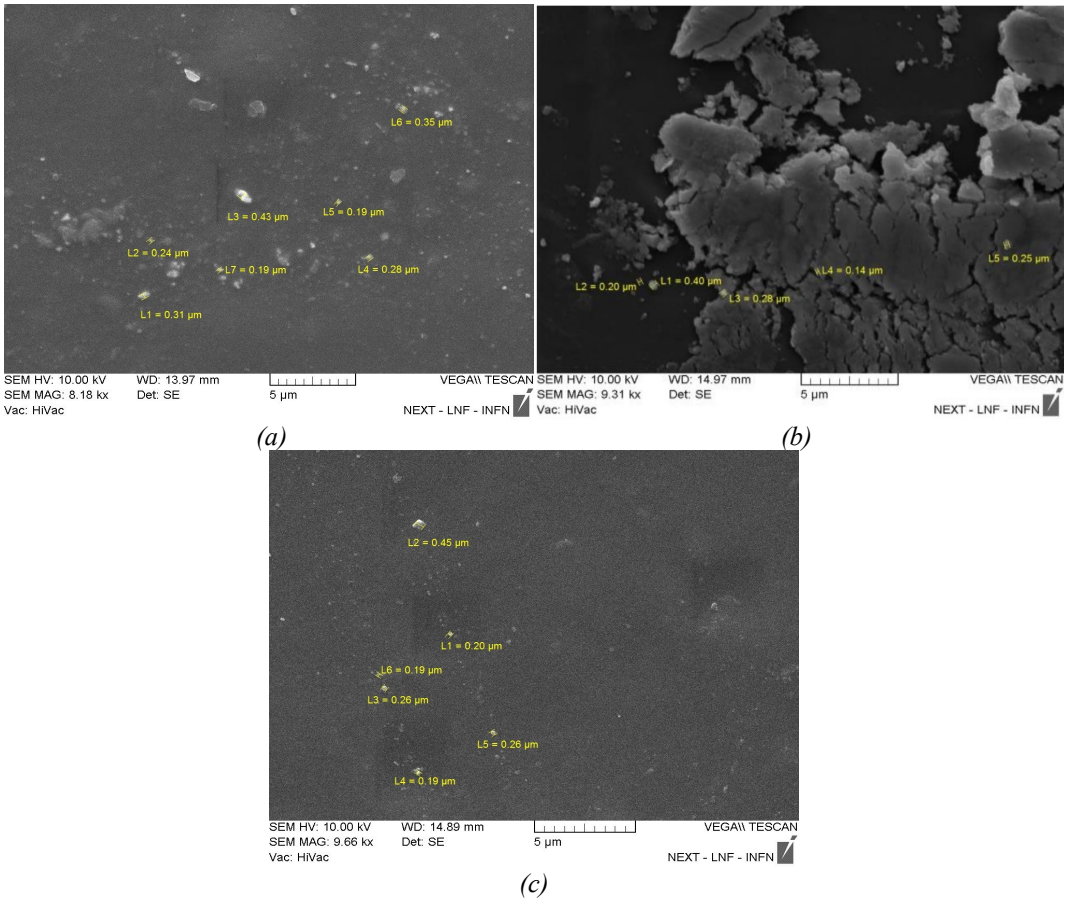

Fig. 10. SEM images of 20% GO/PVA Composite: a) at 40°C; c) at 70°C; d) at 110°C.

4. Conclusions

Using the Hummer method, GO was effectively synthesized and GO/PVA nanocomposite materials were prepared at three distinct concentrations: 2%, 3%, and 20%. After being thermally annealed at 40, 70, and 110° C, the nanocomposite materials' characteristics were examined. The PVA polymer matrix softens as temperature rises, and the polymer melts at higher temperatures. New orientations are created when GO penetrates between PVA layers during thermal annealing at 40°C and 70°C. As the temperature rises to 110°C, GO in its basic state decreases, leading to less space between the sheets. As a result, the melted PVA is removed from between its sheets by the GO that developed between the PVA layers at earlier temperatures.

According to Raman measurements, the I_D/I_G ratio for 2% and 3% GO/PVA composite materials increased with increasing temperature compared to the pristine GO. It indicates that the defect in the structure increases due to the effect of temperature. From FTIR measurements, as the amount of GO in the composite material increased, the intensities of the bands decreased which was linked to PVA. In contrast, some peaks completely disappeared at the highest concentration (20%). Based on these results, for all samples, there was no notable variation in band locations as the temperature increased. As the temperature increased during the examination of the sample morphology, it was noted that both large- and small-sized nanoparticles were produced, changing the surface structure of the PVA polymer matrix.

References

[1] Duan, Y., Stinespring, C. D., & Chorpening, B. (2015), Chemistry Open, 4(5), 642-650; https://doi.org/10.1002/open.201500074.
[2] Sandhu IS, Chitkara M, Rana S, Dhillon G, Taneja A, Kumar S., Optical and Quantum Electronics. 2020 Jul;52(7):359; https://doi.org/10.1007/s11082-020-02473-8
[3] Goumri, M., Venturini, J. W., Bakour, A., Khenfouch, M., Baitoul, M. (2016), Applied Physics A, 122(3); https://doi.org/10.1007/s00339-016-9725-3.
[4] Yumura T., Yamasaki A., Phys. Chem. Chem. Phys. 2014;16:9656–9666; https://doi.org/10.1039/C4CP00658E.
[5] Abid, Sehrawat, P., Islam, S. S., Mishra, P., & Ahmad, S. (2018), Scientific reports, 8(1), 3537; https://doi.org/10.1038/s41598-018-21686-2.
[6] Jin Y, Zheng Y, Podkolzin SG, Lee W., Journal of Materials Chemistry C. 2020;8(14):4885-94; https://doi.org/10.1039/C9TC07063J
[7] Sedki M, Mirabedini PS, Nakama K, Stephens G, Groves M, Lee I, Neupane MR, Mulchandani A., Carbon. 2022 Jan 1;186:437-51; https://doi.org/10.1016/j.carbon.2021.10.011
[8] Ghosh, T. N., Pradhan, S. S., Sarkar, S. K., Bhunia, A. K. 2021, Journal of Materials Science: Materials in Electronics, 32(14), 19157-19178; https://doi.org/10.1007/s10854-021-06435-y.
[9] Morimune, S.; Nishino, T.; Goto, T., Polym. J. 2012, 44, 1056–1063; https://doi.org/10.1038/pj.2012.58
[10] Zhao, Y.; Terai, W.; Hoshijima, Y.; Gotoh, K.; Matsuura, K.; Matsumura, K., Appl. Sci. 2018, 8, 2272; https://doi.org/10.3390/app8112272
[11] Yang, W., Deng, X., Huang, W., Qing, X., Shao, Z. (2019), Journal of Oncology, 2019; https://doi.org/10.1155/2019/7254534.
[12] Gong, K., Hu, J., Cui, N., Xue, Y., Li, L., Long, G., Lin, S., 2021, Mater. Des. 211, 110170; https://doi.org/10.1016/j.matdes.2021.110170.
[13] Alptoğa Ö., Uçar N., Yavuz N.K., Önen A., Int. J. Mater. Metall. Eng. 2017;11:430–433; https://doi.org/10.5281/zenodo.1130531.
[14] Bao, C., Guo, Y., Song, L., Hu, Y. (2011), Journal of Materials Chemistry, 21(36), 13942; https://doi.org/10.1039/c1jm11662b.
[15] Dangi SB, Hashmi SZ, Kumar U, Choudhary BL, Kuznetsov AE, Dalela S, Kumar S, Dolia SN, Kumar S, Sofi BF, Darwesh R., Diamond and Related Materials. 2022 Aug 1;127:109158; https://doi.org/10.1016/j.diamond.2022.109158
[16] Das L, Das P, Bhowal A, Bhattachariee C., Environmental technology & innovation. 2020 May 1;18:100664; https://doi.org/10.1016/j.eti.2020.100664
[17] Qing W, Li X, Wu Y, Shao S, Guo H, Yao Z, Chen Y, Zhang W, Tang CY., Journal of membrane science. 2020 Oct 15;612:118476; https://doi.org/10.1016/j.memsci.2020.118476
[18] Zhong Q, Shi G, Sun Q, Mu P, Li J., Journal of Membrane Science. 2021 Dec 15;640:119836; https://doi.org/10.1016/j.memsci.2021.119836
[19] Hu, X., Ren, N., Wu, Y., Jin, L., Chen, S., & Bai, Y. (2023), Journal of Polymer Engineering, 43(2), 135-143; https://doi.org/10.1515/polyeng-2022-0114.
[20] Abu Hurayra-Lizu, K.M.; Bari, M.W.; Gulshan, F.; Islam, M.R., Heliyon 2021, 7, e06983; https://doi.org/10.1016/j.heliyon.2021.e06983.
[21] Kashyap S, Pratihar SK, Behera SK., Journal of Alloys and Compounds. 2016 Nov 5;684:254-60; https://doi.org/10.1016/j.jallcom.2016.05.162
[22] Gahramanli, L., Muradov, M., Eyvazova, G., Baghirov, M. B., Mammadyarova, S., Aliyeva, G., Bellucci, S. (2023), ChemEngineering, 7(5), 92; https://doi.org/10.3390/chemengineering7050092.
[23] Muradov, M., Baghirov, M. B., Eyvazova, G., Gahramanli, L., Mammadyarova, S., Aliyeva, G., Abdullayev, M. (2023), Radiation Physics and Chemistry, 208, 110926; https://doi.org/10.1016/j.radphyschem.2023.110926.
[24] Baghirov MB, Muradov M, Eyvazova G, Mammadyarova S, Gahramanli L, Aliyeva G, Huseynov E, Abdullayev M., RSC advances. 2023;13(50):35648-58; https://doi.org/10.1039/D3RA07186C

[25] Hieu, N. H., Long, N. H. B. S., Kieu, D. T. M., Nhiem, L. T. (2016), Journal of Electronic Materials, 45, 2341-2346; https://doi.org/10.1007/s11664-015-4281-8.
[26] Wu, X.; Xie, Y.; Xue, C.; Chen, K.; Yang, X.; Xu, L.; Zhang, D., Mater. Res. Express 2019, 6, 075306; https://doi.org/10.1088/2053-1591/ab11ee.
[27] Badrinezhad, L., Bilkan, Ç., Azizian-Kalandaragh, Y., Nematollahzadeh, A., Orak, I., Altindal, S¸ 2018, Int. J. Mod. Phys. B 32, 1750276; https://doi.org/10.1142/S0217979217502769.
[28] Theophile, N., Jeong, H. K. (2017), Chemical Physics Letters, 669, 125-129; https://doi.org/10.1016/j.cplett.2016.12.029.
[29] Mohamed, E. F., Mohamed, F., El-Mekawy, A., El Hotaby, W. (2023); Journal of Inorganic and Organometallic Polymers and Materials, 1-13; https://doi.org/10.1007/s10904-023-02762-1
[30] Sujiono, E.; Zurnansyah; Zabrian, D.; Dahlan, M.; Amin, B.; Samnur; Agus, J., Heliyon 2020, 6, e04568; https://doi.org/10.1016/j.heliyon.2020.e04568.
[31] Yoo, M.J.; Park, H.B., Carbon 2019, 141, 515–522; https://doi.org/10.1016/j.carbon.2018.10.009.
[32] Bhatnagar, D.; Singh, S.; Yadav, S.; Kumar, A.; Kaur, I., Mater. Res. Express 2017, 4, 015101; https://doi.org/10.1088/2053-1591/4/1/015101
[33] Guerrero-Contreras, J.; Caballero-Briones, F., Mater. Chem. Phys. 2015, 153, 209–220; https://doi.org/10.1016/j.matchemphys.2015.01.005
[34] Mehdinavaz Aghdam, R., Yazdanpanah, M., Khanmohammadi, M. R. K., Azami Ghadikolayi, M., Ghelich, R., Shaabani, K., Babaei, M. (2015), Scientia Iranica, 22(6), 2756-2765.
[35] Liao, G. M., Yang, C. C., Hu, C. C., Pai, Y. L., Lue, S. J. (2015), Journal of membrane science, 485, 17-29; https://doi.org/10.1016/j.memsci.2015.02.043
[36] Tzounis, L.; Kirsten, M.; Simon, F.; Mäder, E.; Stamm, M., Carbon 2014, 73, 310–324; https://doi.org/10.1016/j.carbon.2014.02.069
[37] Goumri M, Venturini JW, Bakour A, Khenfouch M, Baitoul M., Applied Physics A. 2016 Mar;122(3):212; https://doi.org/10.1007/s00339-016-9725-3
[38] Wang, T., Li, Y., Geng, S., Zhou, C., Jia, X., Yang, F., Yang, H. (2015), RSC advances, 5(108), 88958-88964; https://doi.org/10.1039/C5RA16158D
[39] Jipa, I. M., Stoica, A., Stroescu, M., Dobre, L. M., Dobre, T., Jinga, S., Tardei, C. (2012), Chemical Papers, 66, 138-143; https://doi.org/10.2478/s11696-011-0068-4
[40] Korbag, I., & Mohamed Saleh, S. (2016), International Journal of Environmental Studies, 73(2), 226-235; https://doi.org/10.1080/00207233.2016.1143700
[41] Kumar, N., Das, S., Bernhard, C., Varma, G. D. (2013), Superconductor Science and Technology, 26(9), 095008; https://doi.org/10.1088/0953-2048/26/9/095008
[42] Emiru, T. F., & Ayele, D. W. (2017), Egyptian Journal of Basic and Applied Sciences, 4(1), 74-79; https://doi.org/10.1016/j.ejbas.2016.11.002
[43] Peng, X., He, C., Liu, J., & Wang, H. (2016), Journal of Materials Science, 51(12), 5901–5911; https://doi.org/10.1007/s10853-016-9891-x
[44] M. Alkan, R. Benlikaya, J. Appl. Polym. Sci. 112, 3764–3774 (2009); https://doi.org/10.1002/app.29830
[45] V.V. Vodnik, Z. Saponjic, U. Bogdanović, J.M. Nedeljković, Mater. Res. Bull. 48, 52–57 (2013); https://doi.org/10.1016/j.materresbull.2012.09.059
[46] Martin, M., Prasad, N., Sivalingam, M. M., Sastikumar, D., Karthikeyan, B. (2017), Journal of Materials Science: Materials in Electronics, 29(1), 365–373; https://doi.org/10.1007/s10854-017-7925-z
[47] Jabbar, W. A., Habubi, N. F., Chiad, S. S. (2010), Journal of the Arkansas Academy of Science, 64(1), 101-105.